19

Life Assessment of a Balloon-Expandable Stent for Atherosclerotic Renal Artery Stenosis

Hao-Ming Hsiao[1], Michael D. Dake, MD[2],
Santosh Prabhu[3], Mahmood K. Razavi, MD[4],
Ying-Chih Liao[5] and Alexander Nikanorov, MD[3]
[1]*National Taiwan University, Department of Mechanical Engineering, Taipei*
[2]*Stanford University, Department of Cardiothoracic Surgery, Stanford, CA 94305*
[3]*Abbott Laboratories, Abbott Vascular, Santa Clara, CA 95054*
[4]*St. Joseph Vascular Institute, Orange, CA 92868*
[5]*National Taiwan University, Department of Chemical Engineering, Taipei*
[1,5]*Taiwan*
[2,3,4]*USA*

1. Introduction

A stent is a small wire-mesh tube that can be deployed into a blood vessel and expanded using a small balloon (or self-expanded) during angioplasty to open a narrowed blood vessel. The expanded stent exerts radial force against the walls of the artery, thereby preventing reclosure of the artery. The scaffolding provided by the stent can also help prevent small pieces of plaque from breaking off and traveling downstream to cause major events such as stroke in distal organs.

Atherosclerotic Renal Artery Stenosis (RAS) is a common manifestation of generalized atherosclerosis and the most common disorder of the renal arterial circulation. Untreated renal artery stenosis can lead to progressive hypertension, renal insufficiency, kidney failure, and increased mortality. Despite the proven efficacy of traditional surgical procedures such as endarterectomy and renal artery bypass, endovascular therapy has emerged as an effective strategy for treatment. Renal angioplasty and endoluminal stenting are performed at an increasing rate, especially in patients with the most complex form of the disease (Blum et al., 1997; Zeller et al., 2003). Balloon-expandable stenting for aorta-ostial renal artery stenosis has been demonstrated to be a safe and effective therapy (Rocha-Singh et al., 2005). It offers more permanent relief to patients without lifelong prescription for medications or surgical procedure. Figure 1 shows the Computed Tomography Angiography (CTA) of the stented left renal artery with severe calcification. A longitudinal image cut through the aorta and the stented left renal artery reveals the cross section of stent struts and the extent of calcification around the renal artery wall.

During normal breathing, the kidneys move up and down due to the diaphragm motion and the renal arteries subsequently experience bending at or close to the point of fixation to the aorta. Figure 2 shows the angiograms of the kidney and the renal artery motion during respiration. Figure 3 shows their motion using a guidewire and a catheter for tracking. It is unclear what impact this kidney motion has on stents implanted in renal arteries. This kidney/arterial motion is important in the evaluation of patients receiving balloon-

expandable stents in order to understand potential risks of stent fractures or in-stent restenosis associated with renal stenting (stent fracture may trigger intimal hyperplasia leading to restenosis). This raises the question of whether the motion of the kidneys and subsequent bending of the arteries would negatively impact balloon-expandable stent fatigue life and cause stent fractures?

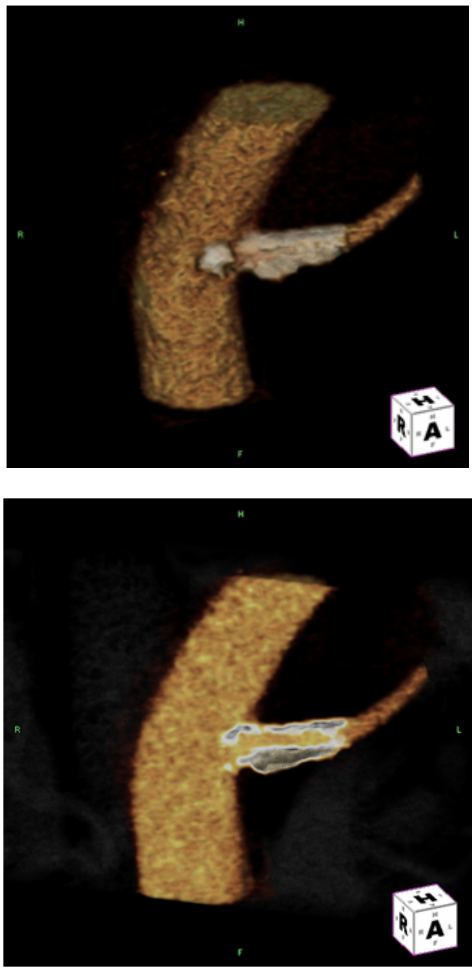

Fig. 1 (a, b) Computed Tomography Angiography of the stented left renal artery with severe calcification, (a) CTA 3D reconstructed image, (b) longitudinal cut through the aorta and the stented left renal artery

Although stent fractures in various vascular and nonvascular beds may not necessarily threaten the patients' life, it is an undesirable event that should be avoided if possible. A literature review revealed that stent fractures have been observed in renal arteries. Bessias et al. reported stent thrombosis in a 47-year-old patient with a single kidney and diseased renal artery who underwent implant of a balloon-expandable stent (Bessias et al., 2005). The

patient presented 25 days after the procedure with renal insufficiency and uncontrolled hypertension. Angiography showed a thrombosed stent which required an aortorenal bypass. The explanted renal artery revealed a fractured incompletely-expanded stent. Similarly, Sahin et al. observed a fractured stent in a 55-year-old patient with mobile kidney (Sahin et al., 2005). They observed fracture of the stent resulted from mobility of the left kidney and suspected that the intimal hyperplasia the patient had 2 months after stenting was triggered by inflammatory reaction at the stent fracture points due to destruction and irritation of the vessel wall. The former case report underscores the possibility of "missed" fractures in balloon-expandable stents that could lead to restenosis and/or thrombosis and the latter points to a possible mechanism. Stent fractures in renal arteries are difficult to identify and may be missed if they are not carefully looked for.

Earlier studies investigated the impact of respiration-induced motion of the kidneys for the purpose of radiotherapy planning to accurately treat tumors. It was reported that the kidneys moved approximately 20-40 mm in the craniocaudal dimension during normal respiration, but provided limited quantitative information on the renal artery movement. Additionally, Magnetic Resonance Imaging (MRI) revealed that displacements of the left and right kidney during normal respiration varied from 2 to 24 mm and 4 to 35 mm, respectively (Moerland et al., 1994). Forced respiration (maximal inspiration and expiration) displacement of the left and right kidney varied from 10 to 66 mm and 10 to 86 mm, respectively. The maximal vertical motion of 39 mm for the superior pole and 43 mm for the inferior pole was reported in another MRI study (Schwartz et al., 1994).

A recent study (Draney et al., 2005) evaluated not only the kidney movement but also the displacement and bending of the renal arteries during respiration using enhanced Magnetic Resonance Angiography (MRA) in healthy male volunteers. The left and right kidneys were displaced 10.1 mm and 13.2 mm, respectively. It was found that the renal ostia were relatively fixed with the displacement of 10-fold less than that of the kidneys. The differential in displacement between the renal ostia and the kidneys resulted in statistically significant changes in renal branch angle. The branches exhibited a greater branch angle at inspiration and were more perpendicular at expiration.

In the current medical device industry, most of the coronary and endovascular stents are assessed using accelerated in-vitro fatigue testing and Finite Element Analysis (FEA) to ascertain whether the device will survive a fatigue life of ten years under simulated physiological loading conditions. To design against such fatigue failures, the majority of prior research on stent fatigue was focused on determining the stress/strain-life (*S-N*) properties of wires and stents (Harrison & Lin, 2000; Pelton et al., 2003; Wagner et al., 2004).

Marrey et al. developed a new damage–tolerant analysis for quantitatively predicting the fatigue life of a balloon-expandable stent (Marrey et al., 2006). Their approach was to base the primary fatigue-life assessment on a traditional, yet conservative version of an *S-N* analysis, and to further use fracture mechanics in order to evaluate the role of pre-existing flaws. Similar work was extended to the nickel-titanium stents for endovascular applications (Robertson & Ritchie, 2007).

Hsiao et al. presented the first evaluation of the impact of the kidney motion on the renal stent fatigue performance (Hsiao et al., 2007 & 2009). It was concluded that the fatigue performance of the studied balloon-expandable stent is excellent under cardiac pulsatile fatigue alone, but compromised to certain degrees when respiration-induced renal artery bending fatigue was also considered. The change in bending angle was more significant for the overlapped stent configuration, resulting in lower fatigue performance when compared to the implant of only one single stent. The following strategy was employed during the study:

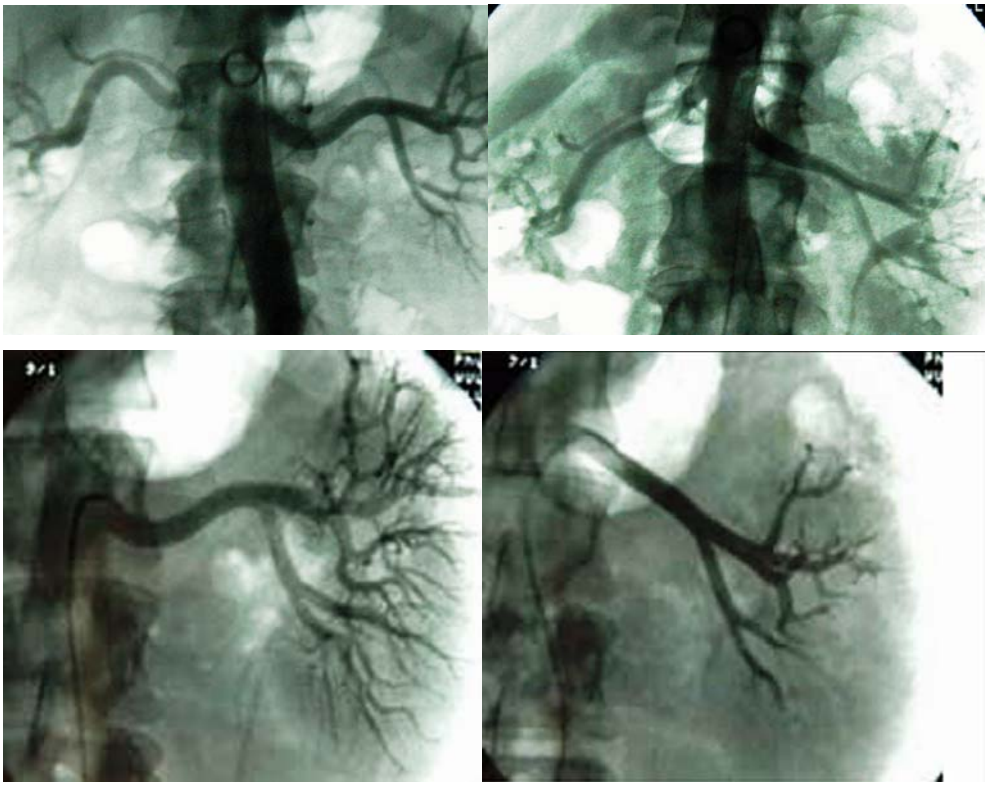

Fig. 2. (a, b) Angiograms showing the kidney and the renal artery motion during respiration, (a) expiration (kidneys moving up), (b) inspiration (kidneys moving down)

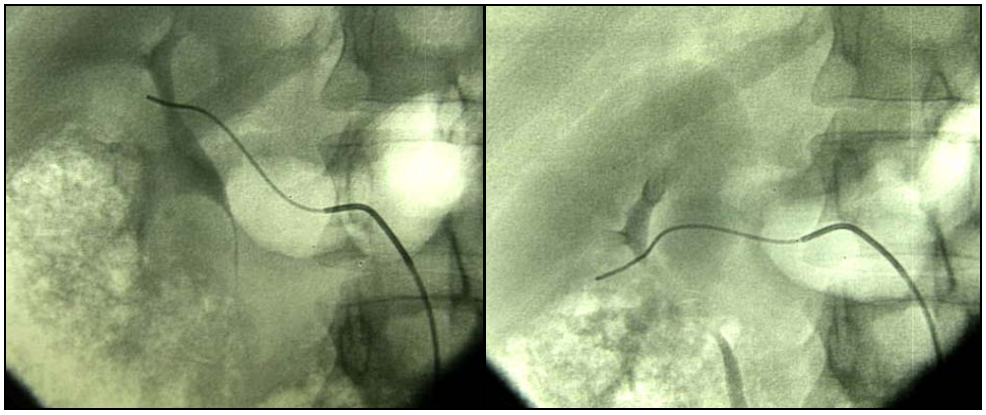

Fig. 3. (a, b) Fluorograms recorded during the right renal artery catheterization demonstrating the kidney and the renal artery motion during respiration by tracking a guidewire and a catheter placed in the renal artery, (a) expiration, (b) inspiration

1. Fluoroscopic images of the stented renal arteries were taken from cadavers at simulated inspiration/expiration positions. Respiratory motion was simulated by manual manipulation of the kidneys to reflect their craniocaudal movement observed clinically.
2. Stent bending during simulated respiration was measured from fluoroscopic images and used as input parameters for the subsequent finite element model.
3. Finite element analysis was performed to assess the balloon-expandable stent bending fatigue performance during respiration.

2. Cadaveric model study

A newly developed L-605 cobalt-chromium balloon-expandable stent was used in this study (Fig. 4). The use of the cobalt-chromium material enables reduction of the stent's wall thickness relative to traditional stainless steel to improve the stent's hemodynamic properties while retaining adequate visibility under fluoroscopy. Figure 5 shows the radiopacity comparison between this new cobalt-chromium stent and its stainless-steel counterpart. It appears that the cobalt-chromium stent has higher radiopacity than the stainless-steel stent. The stent was designed to form a series of nested rings interconnected with small bridging connectors. The design parameters such as crown (or apex) radius and strut dimension were tailored to optimize the stent performance. The unique stent design provides excellent flexibility and low profile to allow physicians' easy device delivery. The stent family covers the nominal stent inner diameters from 4 to 7 mm. In clinical use, the stent may be post-expanded to 1 mm greater than the nominal diameter if necessary. The stents were processed by laser cutting the intended design pattern onto the surface of the hypotube, the starting tube for the manufacture of intravascular stents and other biomedical devices. The as-cut stent surfaces were then electrochemically polished to achieve a good surface finish (Fig. 6).

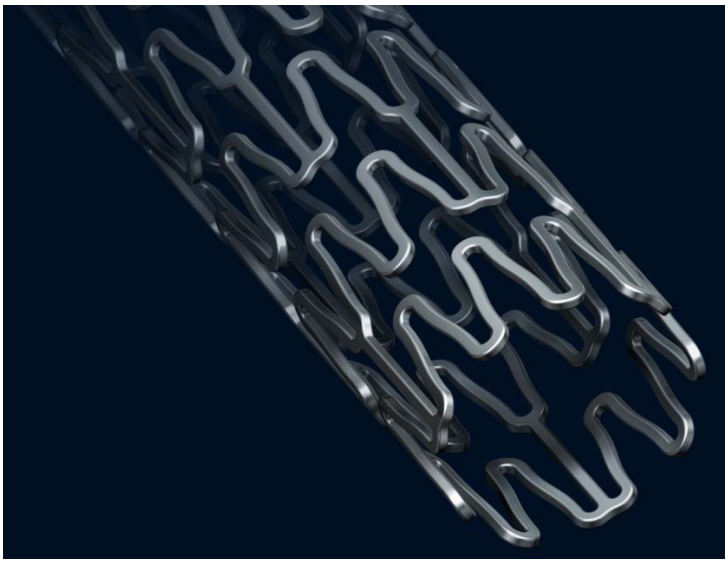

Fig. 4. Newly designed cobalt-chromium balloon-expandable stent used in this study

To test this balloon-expandable stent not yet approved for clinical use at the time of this work, a cadaveric study was performed where two cadavers (henceforth designated as Cadaver A, Cadaver B) were used. Both cadavers were middle-aged individuals, one male and one female. Their cause of death in both cases was unrelated to cardiovascular diseases. The cadavers were prepared based on the methods developed by Garrett (Garrett, 2001) to allow warm (body temperature) saline through the vasculature to simulate blood flow and maintain lumen pressure. The artery lumen was pressurized with saline during renal artery catheterization and stent deployment. Each cadaver was placed in the supine position. To implant stents, endovascular access to the renal arteries was obtained via the femoral artery. The first 7 x 18 mm stent was deployed into the renal arteries of two cadavers through a transfemoral approach such that the end of the stent completely covered the renal ostium where the lesion is usually located. The stent was expanded to 7 mm (inner diameter) and then post-expanded slightly.

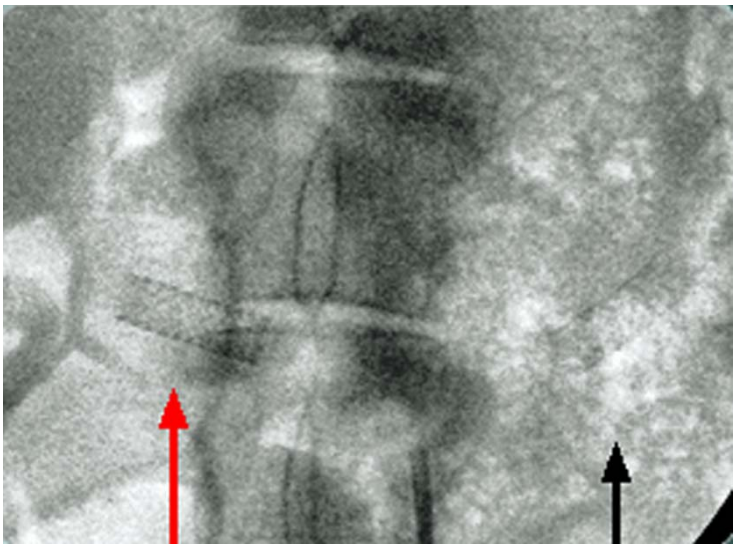

Fig. 5. Radiopacity comparison between the studied cobalt-chromium stent (left) and its stainless-steel counterpart (right)

Surgical access to the abdominal cavity and retroperitoneal space was then obtained via the midline incision through the abdominal wall. Contents of the abdominal cavity were partially removed to allow access to the renal arteries and kidneys. Mineral oil was used to lubricate the tissues of the body cavities and inside the renal arteries to ensure ease movement of tissues against each other. Sutures were sewn to the tissues surrounding the renal arteries and umbilical tape was looped around the renal arteries at the midpoint to facilitate manual manipulation and displacement of the kidneys. It should be noted that, although saline was continuously pumped into the vasculature during procedure, lumen pressure dropped due to saline leaking through the small arterial branches after surgical exposure of the kidneys and renal arteries. Respiratory movement was simulated by manual manipulation of the kidneys (Fig. 7). The displacement of the kidneys was estimated to be 40 mm based on the clinical human data. The stents were implanted when

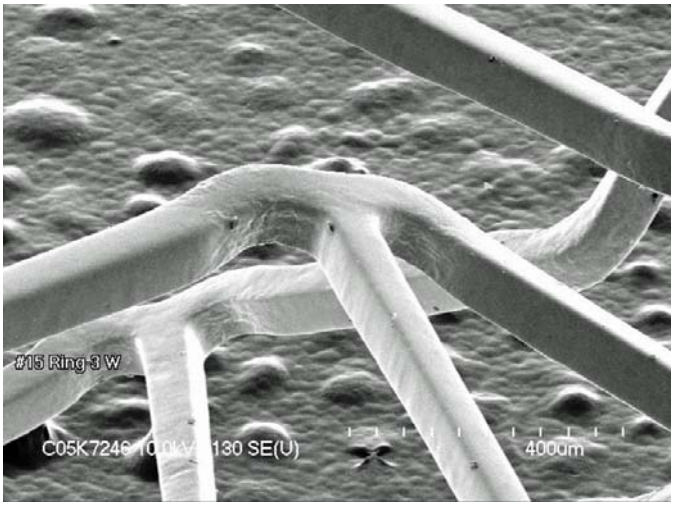

Fig. 6. Scanning Electron Microscopy (SEM) image of the studied cobalt-chromium stent showing a good surface finish after electrochemical polishing

kidneys were in the neutral position. The displacements of +20 mm cranial (towards head for expiration simulation) and -20 mm caudal (towards legs for inspiration simulation) from the kidney were measured with a ruler to establish the upper and lower bounds of the kidney movement. The manual simulation of the kidney movement was attempted in such a way that the kidney movement plane was considered close to perpendicular to the plane of view. Therefore, it is believed that the measurements were able to capture the true bending angle changes. The guide wire tip position, C-Arm (X-ray mobile diagnostic machine) floor position, and cadaver position remained unchanged throughout each cycle of one simulated inspiration and expiration movement to ensure consistency of the reference points. Fluoroscopic images were collected for later analysis.

After implanting the first stent, a second stent was deployed into the renal arteries of two cadavers such that the proximal portion of the second stent overlapped the distal portion of the first stent by approximately 3-4 mm. This was to simulate a potentially worst case clinical scenario. Respiration motion was again simulated by manual manipulation of the kidneys and fluoroscopic images were collected. Figure 8 shows the explanted and opened aortic segment with two overlapped stents implanted in the renal artery.

3. Finite element analysis

Stents placed in the vasculature are subjected to various modes of cyclic loading that may consequently compromise the structural integrity of the stents during their functional life resulting in fatigue failure. In this study, Finite Element Analysis (FEA) was performed to evaluate the stent structural integrity and fatigue performance. Simulation was performed to ensure whether the stent will survive 4×10^8 cycles under simulated physiological environment with a combination of cardiac pulsatile fatigue loading and respiratory bending fatigue loading. Ten years of fatigue life, accepted as a standard for stents today, is equivalent to 4×10^8 cardiac systolic/diastolic cycles and approximately 0.5×10^8 - 1×10^8 respiratory cycles (assuming human breath rate is 10-20 times per minute). Therefore, the

combined cardiac pulsatile and respiratory bending fatigue simulation (4 x 10^8 cycles for each) performed in this study represents a far more conservative assessment to the studied stent fatigue performance. The fatigue mean stress of 1689 MPa was obtained at Abbott Vascular using the Instron mechanical testing machine in accordance with the procedures outlined in ASTM E8-98, ASTM E83-96, and ASTM E345-93. The test procedure involved standard tensile strength testing of the L-605 cobalt-chromium tubing using extensometers for strain measurements. The fatigue alternating stress of 483 MPa was obtained from the material supplier and verified by literature publications (Bjork, 1985).

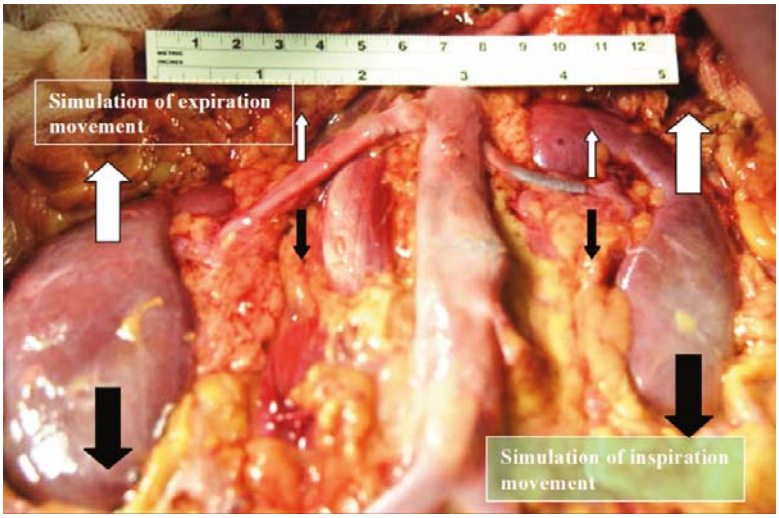

Fig. 7. Simulation of the kidney and the stented renal artery motion during the respiratory cycle

A finite element model was developed to evaluate the stent response to various loading conditions involved in preparing and deploying an intravascular stent consistent with clinical practice such as manufacturing (crimped onto a balloon catheter), *in vivo* deployment (expanded into an artery), and clinical vascular environment (systolic/diastolic pressure, respiration-induced bending). The stent fatigue analysis determined the state of stress and strain due to loading imposed by the following procedure:

Step 1. Stent crimping from 2.54 mm to 1.36 mm OD
Step 2. Stent recoil after crimping
Step 3. Stent expansion to 7.0 mm ID
Step 4. Stent recoil after expansion
Step 5. Stent bending during inspiration superimposed with systolic/diastolic pressure (180/80 mmHg)
Step 6. Stent bending during expiration superimposed with systolic/diastolic pressure

In order to evaluate the stent long-term fatigue performance under the loading conditions imposed by inspiration and expiration along with the systolic and diastolic arterial blood pressure loading, a Goodman fatigue analysis was performed using the multi-axial stress state experienced in Step 5 and 6. Since the stent is diametrically over-expanded relative to the vessel, there is a significant compressive preload imposed on the stent that results in

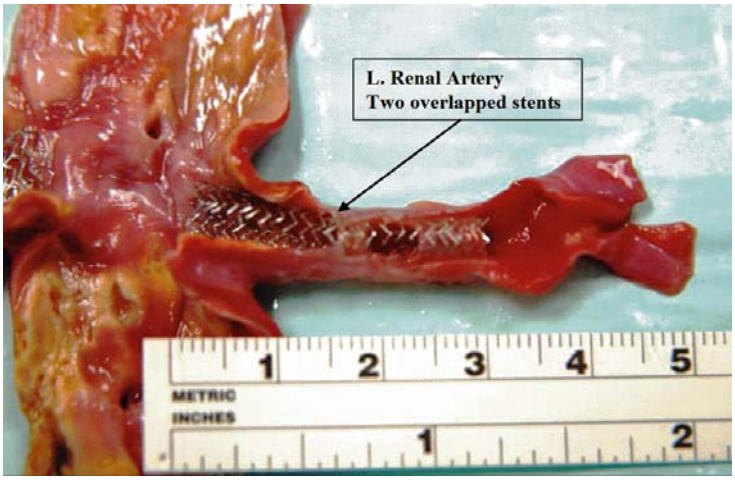

Fig. 8. Partially exposed explanted aortic segment with the left renal artery demonstrating position of the implanted overlapped stents

fatigue cycling with a mean stress not equal to zero. It should be noted that mean stress could also be a result of the plastic deformations of crimping and deployment. The Goodman relation states that fatigue failure will occur if the stress state in the component satisfies the relation:

$$\left(\frac{\sigma_a}{\sigma_e}\right)+\left(\frac{\sigma_m}{\sigma_u}\right)\geq 1 \tag{1}$$

where σ_a is the stress amplitude applied to the component, σ_e is the modified material endurance limit for non-zero mean stress, σ_m is the mean stress applied to the component, and σ_u is the material ultimate stress. The Goodman fatigue analysis was performed using the following effective mean stress and effective stress amplitude equations:

$$\sigma_m=\frac{1}{\sqrt{2}}\sqrt{(\sigma_{1m}-\sigma_{2m})^2+(\sigma_{2m}-\sigma_{3m})^2+(\sigma_{3m}-\sigma_{1m})^2} \tag{2}$$

$$\sigma_a=\frac{1}{\sqrt{2}}\sqrt{(\sigma_{1a}-\sigma_{2a})^2+(\sigma_{2a}-\sigma_{3a})^2+(\sigma_{3a}-\sigma_{1a})^2} \tag{3}$$

where σ_m is the effective mean stress, σ_a is the effective stress amplitude, σ_{1m}, σ_{2m}, σ_{3m} are the principal mean stresses, and σ_{1a}, σ_{2a}, σ_{3a} are the principal stress amplitudes experienced. The principal stresses σ_1, σ_2, σ_3 were first extracted at each integration point for the combined pulsatile and bending loading conditions. These principal stresses were used to calculate the principal mean stresses and stress amplitudes. Once the principal mean stresses and stress amplitudes were determined, the effective mean stress and stress amplitude were then calculated at each integration point using the above equations.

The Fatigue Safety Factor (FSF) is defined as the ratio of the stress amplitude against the modified endurance limit, where the stress amplitude is the stress difference and the mean stress is the average stress on the element stresses. It quantifies the proximity of the mean

stress and stress amplitude at any given numerical integration point to the limiting Goodman curve. The integration points were used instead of nodal points in this study for accuracy and consistency reasons. While the integration points do not allow for recovered surface stresses, they offer the true exact solution without any extrapolation errors associated with nodal values. Fatigue Safety Factor less than 1.0 indicates a fatigue failure.

$$FSF = \frac{\sigma_e}{\sigma_a} \tag{4}$$

The ABAQUS/Standard finite element solver was used to perform the stent fatigue analysis. In order to prevent shear locking induced by bending loads, the stent struts were modeled using C3D8I fully integrated 3D solid elements with incompatible modes. The models were three-layers deep through the thickness and contained six elements in the width dimension to ensure that stress variation was adequately captured (Fig. 9). Mesh density studies of similar problems were performed to select the appropriate mesh density for the representative stress and strain distribution throughout the stent. It was concluded from the studies that the maximum stresses with the selected 6x3 mesh were able to converge within 5% of the true values. The mid-section of the stent was free to deform during crimping and expansion. Contact surfaces were defined at the strut edges to prevent inter-penetration between the struts during the crimping process. Additional contact surfaces were imposed as needed on the outer and inner stent surfaces to provide stent interaction with the crimping and expanding rigid surfaces during the crimping and expansion processes. The analytical rigid surfaces were defined to change in radius with each increment during the simulation. Contact was removed between the stent and the rigid surface during the recoil phases to allow the stent free deformation. The recoil process resulted in the relaxation of elastic strain energy and did not incur any change in the plastic strain distribution. A pressure of 180 mmHg (systolic) and 80 mmHg (diastolic) was used during steps 5-6 to simulate the cyclic fatigue loading applied to the stent by the blood pressure. In order to account for the loading imposed by the arterial wall, the arterial pressure loading corresponding to the interaction between the stent and the artery was imposed on the stent. The bending fatigue model consisted of four stent rings, approximately 1/3 of the single stent length. When two stents are deployed in a tortuous vessel and overlapped, the overlapped section is relatively stiff compared to the other two free ends. Therefore, the overlapped section of the stent was considered to be the fixed end with the non-overlapped section of the stent hanging free. The analytical rigid surface was defined to change in bending curvature during the simulation. The applied bending curvatures to the FEA model were calculated based on the average bending angles measured from fluoroscopic images of the cadaveric study.

4. Results and discussion

4.1 Respiration-induced Stent Bending Angle Measurement

Figures 10 and 11 show the representative fluoroscopic images of the stented renal arteries at simulated inspiration and expiration positions for the single and overlapped stents, respectively. As shown, the stents were subjected to bending during respiration with significant rigid body motion (translation and rotation) involved. Rigid body motion does not contribute to the stent deformation and was therefore ignored in the analysis. It is

interesting to note that, for the single stent configuration, the stented portion of the renal arteries was relatively straight (indicating minor bending), thus pushing the vessel bending distally towards the kidney during expiration. However, for the overlapped stent configuration, the overlapped stents took the bending curvature of the renal arteries smoothly but they were apparently subjected to greater degree of bending.

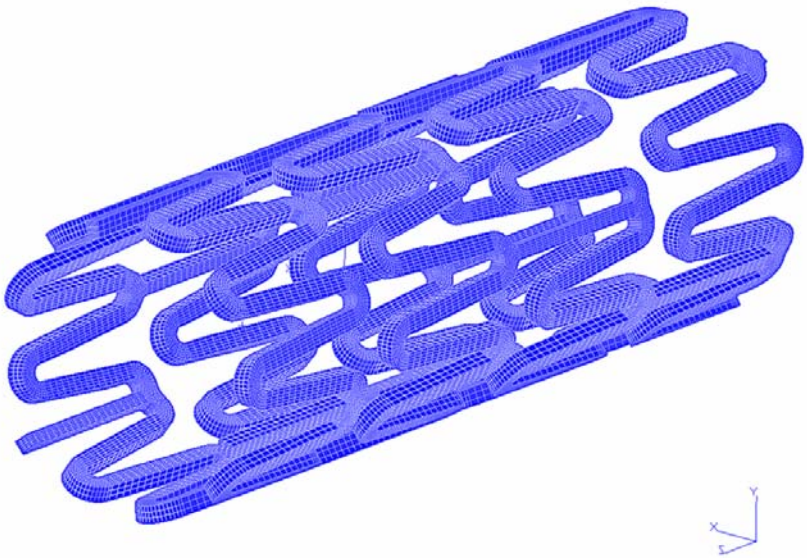

Fig. 9. A 6x3 mesh stent finite element model for combined cardiac pulsatile fatigue and respiratory bending fatigue

Kidney motion during respiration results in bending of the renal arteries, thereby deforming the longitudinal axis of the stent into a curved line. Figure 12a illustrates the deflection curve of a stent subjected to bending. A line tangent to the deflection curve at the stent end forms angle θ to the x-axis which represents the bending angle of the stent. When drawing tangent lines to the deflection curve from both ends, based on analytic geometry, the acute intersection angle of these two tangents is 2θ which is twice the defined bending angle. When the bending curvature is non-uniform along the stent length, the bending angle is defined as θ for one end and ϕ for the other end. As a result, the intersection angle of the two tangents is $\theta + \phi$ instead of 2θ. Procedures to determine the bending angle at the stent ends were:

1. Imported fluoroscopic images to AutoCAD software (AutoCAD LT 2000i).
2. Ignored rigid body motion (both translation and rotation).
3. Drew tangential lines to the deflection curve at the stent ends.
4. Measured the acute intersection angle $\theta + \phi$ of the two tangents.
5. Divided $\theta + \phi$ by 2. This is the average bending angle at the end points of the stent. The average bending angle can be related to the average curvature κ or average radius of curvature κ with the following definition:

$\kappa = 1/\rho = 2$ (average bending angle) / L = $(\theta + \phi)$ / L,
where L is the combined stent length.

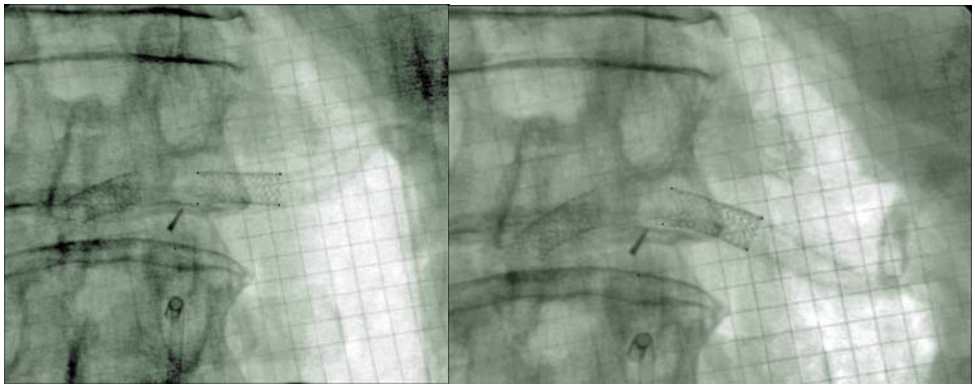

Fig. 10. (a, b) Fluoroscopic images of the stented renal arteries at simulated respiratory positions for the single stent case, (a) expiration, (b) inspiration

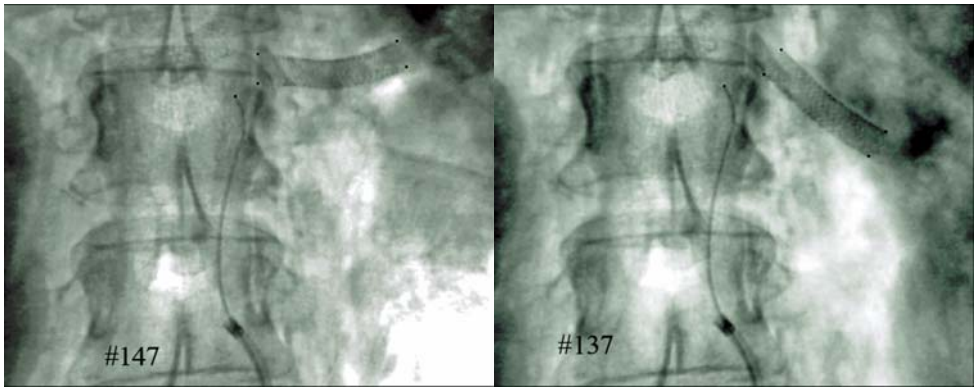

Fig. 11. (a, b) Fluoroscopic images of the stented renal arteries at simulated respiratory positions for the overlapped stent case, (a) expiration, (b) inspiration

The example shown in Figure 12b has the measured acute intersection angle of 20°. In this case, the resulting average bending angle at the stent end is half of that value, 10°, and its corresponding curvature is 0.011 mm^{-1} (radius of curvature: 92 mm). It is interesting to note that, since the intersection point of the two tangents is not at the stent mid point, this implies the stent bending deformation is not uniform.

Table 1 summarizes the average measured bending angle at the stent ends from fluoroscopic images and the calculated bending curvature for both single and overlapped stent cases. As shown, the change in bending angle between inspiration and expiration for the overlapped stent case was approximately 9°, which is considerably greater than the single stent case of 1.7°. The increased bending angle measured at the stent ends of the overlapped stents was partially due to larger bending curvature and partially due to longer overall stent length.

This information was used for the subsequent Finite Element Analysis wherein these bending angles/curvatures were superimposed upon forces associated with high hemodynamic pressure (blood pressure 180/80 mmHg) to simulate conditions achievable in the intended patient population.

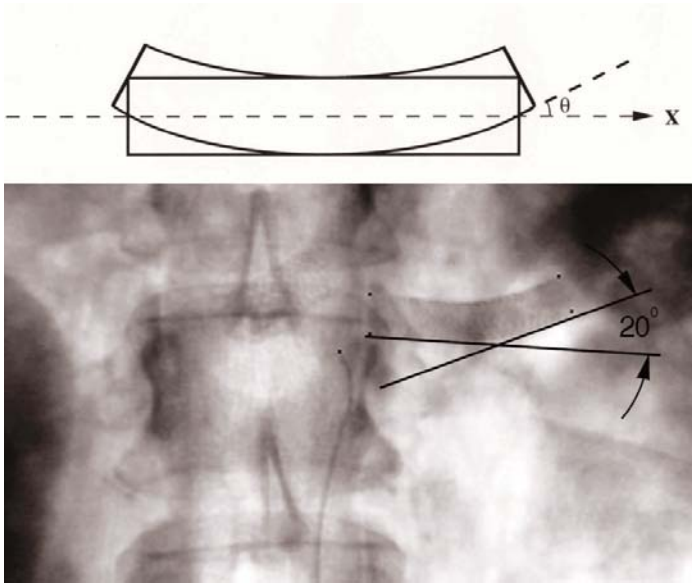

Fig. 12. (a) Deformations of a stent in bending (top), (b) Measured acute intersection angle at expiration (bottom)

	Inspiration		Expiration	
	Bending Angle	Curvature	Bending Angle	Curvature
Single Stent	3.90°	0.008 mm^{-1}	2.20°	0.004 mm^{-1}
Overlapped Stent	2.75°	0.003 mm^{-1}	11.75°	0.013 mm^{-1}

Table 1. Average bending angles and curvatures for the single and overlapped stent cases

4.2 Stent fatigue life

Stents deployed in the single and overlapped configurations were studied. The single stent configuration has been widely used in renal applications, whereas the overlapped stent configuration is to simulate a potential clinical situation where a physician has to deploy two stents overlapping at the ends. An 18 mm long stent, the standard implant size for renal stenting, was used in this study. For the overlapped stent configuration, two 18-mm long stents were overlapped at the stent ends by 3-4 mm, making the total stented renal artery length of approximately 32-33 mm. Although uncommon in renal stenting, this is a common clinical practice in other applications such as in the coronary artery stenting.

Based on the fluoroscopic images of the stented arteries during simulated motion, the single stent and the overlapped stents implanted in the renal arteries behave in a different way during the kidney motion. For the single stent configuration, the stented portion of the renal arteries was relatively short and straight, pushing most of the vessel tortuosity distally towards the kidney (Fig. 10). As a result, the stent was only subjected to minor bending and affected less by kidney motion. However, for the overlapped stent configuration, the longer overlapped stents were forced to conform to the bending curvature of the renal arteries and apparently subjected to a greater degree of bending than the single stent (Fig. 11).

Figures 13-15 show the contour plots of von Mises stress developed during the different steps of the loading process (crimping, expansion, and respiration-induced bending coupled with cardiac pulsatile pressure loading) for the studied balloon-expandable stent. The maximum von Mises stresses and maximum equivalent plastic strains at each loading step occurred on the inner surface of the curved crown "U", "Y", and "W" struts of the model. Figure 14 shows the comparison between FEA simulation and *in-vitro* expansion of the studied stent inside a tube. Results show that the developed FEA model is able to predict the stent expansion geometry very well. Figure 16, an enlargement of struts "U" and "W" at bending, illustrates that the inner surface of the curved crowns experienced high plastic deformation, while the straight links and the curved crown legs were under elastic deformation.

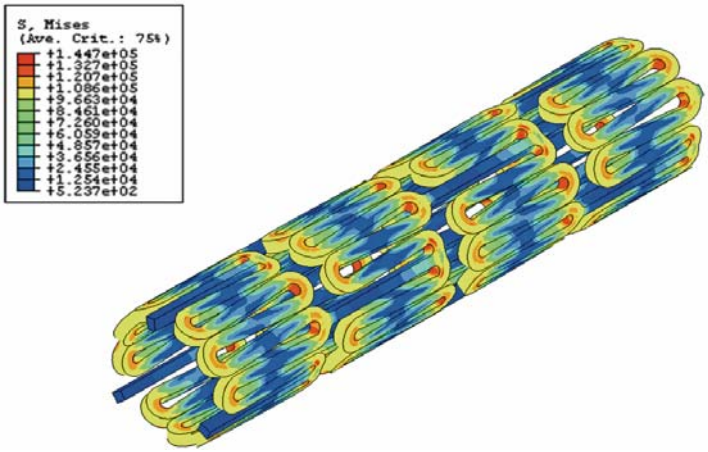

Fig. 13. Contour plots of von Mises stress for the studied balloon-expandable stent at crimping

A Goodman diagram of bending fatigue coupled with pulsatile fatigue is shown in Fig. 17 for the overlapped stent configuration. Calculated data were below the Goodman diagram failure line, indicating the studied balloon-expandable stents in the overlapped configuration are able to pass the fatigue life of 4×10^8 cycles under combined pulsatile and bending fatigue. Comparing Fig. 17b to Fig. 17a where the very same stent was assessed for pulsatile fatigue alone, it is shown that the calculated data of the overlapped stents under combined pulsatile and bending fatigue migrated towards the Goodman diagram failure line, indicating a drop in Fatigue Safety Factor and thus lower fatigue resistance during respiration. This finding also implies that, should longer stents be used clinically in renal applications, more pronounced respiration-induced bending may occur on stents. The degree of bending is likely to increase as the overall stent length becomes longer. The stented portion of the renal artery would become long enough such that it is forced to conform to the curvature the renal artery forms during respiration. Therefore, it is likely that a longer stent or multiple overlapped stents would have a shorter fatigue life than a shorter stent in renal applications. Since most of the renal artery stenosis occurs at the renal ostial region (renal artery and aorta junction), this short region should become the primary focus of the treatment instead of stenting a long section of the renal artery which requires a long stent or multiple overlapped stents.

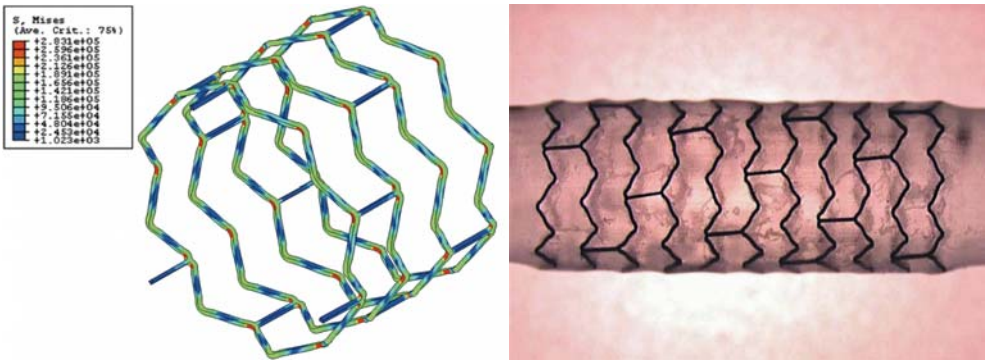

Fig. 14. (a, b) (a) Contour plots of von Mises stress for the studied balloon-expandable stent at expansion, (b) *in-vitro* stent expansion inside a tube

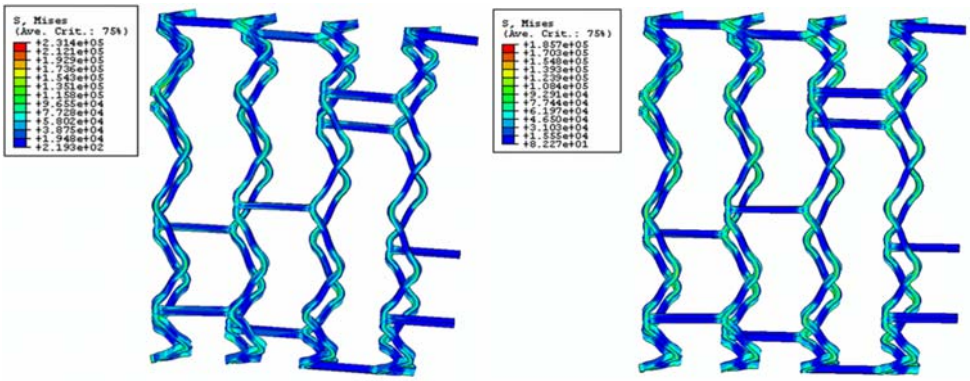

Fig. 15. (a, b) Contour plots of von Mises stress for the studied balloon-expandable stent under respiration-induced bending coupled with cardiac pulsatile pressure loading for the overlapped stent case, (a) expiration, (b) inspiration

It should be noted that the simulated distance between inspiration and expiration (about 40 mm) used in this study represents greater degrees of bending than the actual bending normally seen in the clinical overlapped stent case. The reason for this is that when two stents are overlapped, the entire renal artery becomes stiff enough such that, under similar respiratory forces, the kidney movement may be constrained and thus the movement is not as pronounced as 40 mm observed in other studies during normal breathing with no stents implanted. Therefore, it is hypothesized that the overlapped stent results presented in this paper were considered as the worst case scenario that may be more conservative than the actual.

The stent design also plays a critical role in the stent bending fatigue life. The stent design parameters such as strut width and thickness, crown radius, ring height, and connector number and geometry all have significant impact on the overall stent behavior. When the stent design is less flexible (in contrast to the studied balloon-expandable stent which is very flexible), it tends to straighten out the vessels considerably and pushes the vessel tortuosity distally. This could create kink points at the stent/vessel junctions, which could disturb the

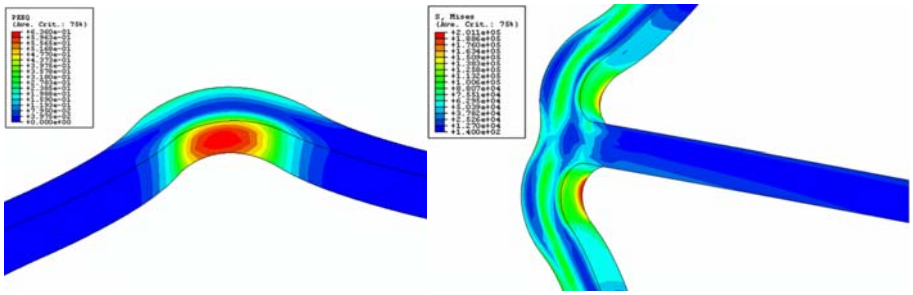

Fig. 16. (a, b) Zoom-in contour plots of the figure 15, (a) maximum strain contour plot at strut U, (b) maximum strain contour plot at strut W

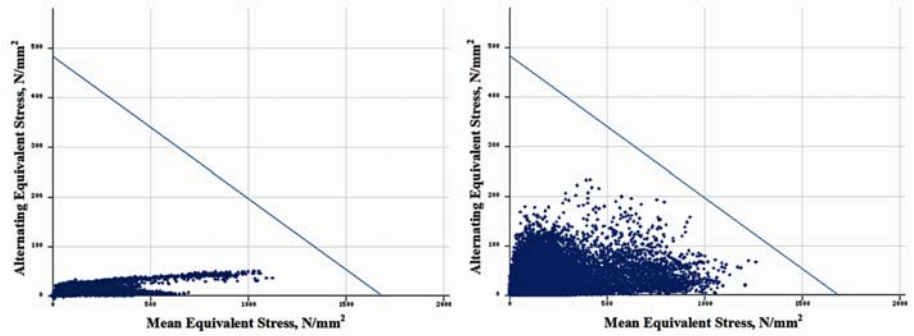

Fig. 17. (a, b) Goodman diagram of the studied balloon-expandable stent for the overlapped stent case, (a) pulsatile fatigue, (b) combined pulsatile and bending fatigue

blood flow and trigger adverse events such as vessel spasm and thrombosis. Such stiffer stent is also likely to have a shorter fatigue life due to the higher stresses created by the stent design itself and its interaction with the surrounding vessel movement. Therefore, it is very important to select the appropriate stent designs for specific applications. For applications subjected to greater degrees of bending such as the renal artery and the superficial femoral artery, a flexible stent design is preferred and should be used. However, for other applications such as carotid stenting where the primary concern is the potential stroke risk of emboli dislodgement from plaque, a stent with greater scaffolding should be considered as the main candidate to help pave the artery better.

5. Conclusion

The purpose of this study was to determine whether the motion of the kidneys during respiration, and subsequent bending of the renal artery, would negatively impact the stent fatigue life. To address this issue, stents were deployed into the renal arteries of two cadavers and respiratory motion was simulated by manual manipulation of the kidneys. Stent bending angles were measured from fluoroscopic images and Finite Element Analysis was performed.

For the single stent configuration, the stented portion of the renal arteries was relatively straight, thus pushing the vessel bending distally towards the kidney. However, for the

overlapped stent configuration, the overlapped stents took the bending curvature of the renal arteries smoothly but they were apparently subjected to greater degree of bending. Measured bending angles and curvatures applied to Finite Element Analysis indicated the stent fatigue resistance became lower and thus the stent life became shorter when the degree of stent bending increased.

This study concluded that the fatigue performance of the studied balloon-expandable stent is excellent under cardiac pulsatile fatigue alone, but compromised to certain degrees when respiration-induced renal artery bending fatigue was also considered. The change in bending angle was more significant for the overlapped stent configuration, resulting in lower fatigue life when compared to the implant of one single stent. Results showed that the studied ballon-expandable stent is not at risk for bending fatigue failure during respiratory motion for both single and overlapped stent configurations. It is strongly recommended that, in addition to the standard cardiac pulsatile fatigue analysis, similar bending fatigue life analysis should be performed on other vascular bed applications such as coronary arteries, carotid arteries, peripheral arteries, etc., in order to ensure the safety and efficacy of the new designed stents.

6. Acknowledgement

This work is supported by National Science Council of Taiwan (NSC 98-2218-E-002-043 and NSC 99-2218-E-002-018) and Abbott Laboratories (Abbott Vascular division). The authors gratefully acknowledge their continued support of the program.

7. References

Bessias, N.; Sfyroeras, G. & Moulakakis, K.G. (2005). Renal Artery Thrombosis Caused by Stent Fracture in a Single Kidney Patient. *Journal of Endovascular Therapy*, Vol. 12, No. 4, pp. 516-520.

Bjork, V.O.; Lindblom, D. & Henze, A. (1985). The Monostrut Strength. *Scand J Thor Cardiovasc Surg*, Vol. 19, pp. 13-19.

Blum, U.; Krumme, B.; Flugel, P.; Gabelmann, A.; Lehnert, T.; Buitrago-Tellez, C.; Schollmeyer, P. & Langer, M. (1997). Treatment of Ostial Renal-Artery Stenoses with Vascular Endoprostheses after Unsuccessful Balloon Angioplasty. *New England Journal of Medicine*, Vol. 336, pp. 459-465.

Draney, M.; Zarins, C.K. & Taylor, C.A. (2005). Three-Dimensional Analysis of Renal Artery Bending Motion During Respiration. *Journal of Endovascular Therapy*, Vol. 12, pp. 380-386.

Garrett, H.E. Jr. (2001). A Human Cadaveric Circulation Model. *J Vasc Surg*, Vol. 33, pp. 1128-1130.

Harrison, W.J. & Lin, Z.C. (2000). The Study of Nitinol Bending Fatigue, *Proceedings of the International Conference on Shape Memory and Superelastic Technologies*, Pacific Grove, CA, April 2000, pp. 391-396.

Hsiao, H.M.; Prabhu, S.; Nikanorov, A. & Razavi, M. (2007). Renal Artery Stent Bending Fatigue Analysis. *ASME J Medical Devices*, Vol. 1, No. 2, pp. 113-118.

Hsiao, H.M.; Nikanorov, A.; Prabhu, S. & Razavi, M. (2009). Respiration-induced Kidney Motion on Cobalt-Chromium Stent Fatigue Resistance. *J Biomed Mater Res Part B: Appl Biomater*, Vol. 91B, No. 2, pp. 508-516.

Marrey, R.V.; Burgermeister, R.; Grishaber R.B. & Ritchie R.O. (2000). Fatigue and Life Prediction for Cobalt-chromium Stents: A Fracture Mechanics Analysis. *Biomaterials*, Vol. 27, pp. 1988-2000.

Moerland, M.A.; van den Bergh, A.C.; Bhagwandien, R.; Janssen, W.M.; Bakker, C.J.; Lagendijk, J.J. & Battermann, J.J. (1994). The Influence of Respiration Induced Motion of the Kidneys on the Accuracy of Radiotherapy Treatment Planning, a Magnetic Resonance Imaging Study. *Radiotherapy and Oncology*, Vol. 30, No. 2, pp. 150-154.

Pelton, A.R.; Gong, X.Y. & Duerig, T.W. (2003). Fatigue Testing of Diamond-shaped Specimens, *Proceedings of the International Conference on Shape Memory and Superelastic Technologies*, Menlo Park, CA, pp. 293-302.

Robertson, S.W. & Ritchie, R.O. (2007). In Vitro Fatigue-crack Growth and Fracture Toughness Behavior of Thin-walled Superelastic Nitinol Tube for Endovascular Stents: A Basis for Defining the Effect of Crack-like Defects. *Biomaterials*, Vol. 28, pp. 700-709.

Rocha-Singh, K.; Jaff, M.R. & Rosenfield, K. (2005). Evaluation of the Safety and Effectiveness of Renal Artery Stenting after Unsuccessful Balloon Angioplasty. *Journal of the American College of Cardiology*, Vol. 46, No. 5, pp. 776-783.

Sahin, S.; Memis, A.; Parildar, M. & Oran, I. (2005). Fracture of a Renal Artery Stent due to Mobile Kidney. *Cardiovascular Interventional Radiology*, Vol. 28, pp. 683-685.

Schwartz, L.H.; Richaud, J.; Buffat, L.; Touboul, E & Schlienger, M. (1994). Kidney Mobility During Respiration. *Radiotherapy and Oncology*, Vol. 32, No. 1, pp. 84-86.

Wagner, M.; Sawaguchi, T.; Kaustrater, G.; Hoffken, D. & Eggler, G. (2004). Structural Fatigue of Pseudoelastic NiTi Shape Memory Wires. *Mater Sci Eng A*, Vol. 378, pp. 105-109.

Zeller, T.; Frank, U.; Muller, C.; Burgelin, K.; Sinn, L.; Bestehorn, H.; Cook-Bruns, N. & Neumann, F. (2003). Predictors of Improved Renal Function after Percutaneous Stent-supported Angioplasty of Severe Atherosclerotic Ostial Renal Artery Stenosis. *Circulation*, Vol. 108, pp. 2244-2249.